Molecular Cell, Volume *31*

Supplemental Data

NMR Solution Structure of the Integral Membrane Enzyme DsbB: Functional Insights into DsbB-Catalyzed Disulfide Bond Formation

Yunpeng Zhou, Tomasz Cierpicki, Ricardo H. Flores Jimenez, Stephen M. Lukasik, Jeffrey F. Ellena, David S. Cafiso, Hiroshi Kadokura, Jon Beckwith, and John H. Bushweller

Supplemental Experimental Procedures

Protein expression and purification. All mutations of DsbB and DsbA were introduced using the QuikChange II XL Site-Directed Mutagenesis Kit (Stratagene). The non-essential Cys residues of DsbB, Cys8 and Cys49, were mutated to Ala and this mutant is referred to as wild-type DsbB throughout the text.

For expression of DsbA, the signal sequence of DsbA was removed and a sequence encoding a "MHHHHHHSSGENLYFQG" tag was attached to the N-terminus of DsbA. The resulting DNA was inserted in the pET22b vector. DsbA was expressed in BL21 (DE3) cells (Novagen) at 37 ºC in minimal medium. Expression was induced with 1.0 mM isopropyl-β-D-thiogalactopyranoside (IPTG) when the OD_{600nm} reached 0.6. Cells

were harvested 6 hours after induction. DsbA was purified using Ni-NTA chromatography, TEV protease cleavage, and a second Ni-NTA chromatography step.

For expression of DsbB, full length DsbB and a sequence encoding a C-terminal "-GHHHHHH" tag was inserted into pET22b (Novagen). The vector was transformed into Rosetta (DE3) cells (Novagen). Cells were cultured in modified M9 minimal medium containing 1% (v/v) of Bioexpress-1000 (Cambridge Isotope Laboratories) at 37 ºC. Expression of DsbB was induced with 10 μM IPTG at an OD_{600nm} of 0.6-0.8. Cells growth was continued at 30 ºC for 4 hours before harvesting.

For purification of DsbB, the cell pellet was resuspended in 50 mM TRIS (pH 8.0), 300 mM NaCl buffer and disrupted by 3 passes through a French press at 18,000 psi. The membrane fraction was pelleted by ultracentrifugation at 100,000g for 1 hour and subsequently resuspended into the same buffer with a Dounce homogenizer. DsbB was extracted from the membrane by adding DPC to a final concentration of 10 g/L followed by gentle rocking at 4 ºC for 0.5 hrs. The insoluble fraction was removed by a second ultracentrifugation step. Solubilized DsbB was purified by Ni-NTA affinity chromatography (Qiagen) with the same TRIS/NaCl buffer containing 1 g/L DPC. Yields of DsbB were between 4 and 8 mg of purified protein per liter of minimal media.

To prepare NMR samples, 7.0 mL of Ni-NTA column elution fraction was concentrated

to 0.3 mL by centrifugal ultrafiltration using an Amicon Ultra-15 Centrifugal Filter Device (5kDa molecular weight cut-off, Millipore). Subsequently, DsbB was exchanged into pH 6.2 buffer (25mM PBS, 50mM KCl, 0.47g/L DPC, 5% (v/v) D_2O) by 3 cycles of 7-fold dilution/concentration.

$^{2}H/^{13}C/^{15}N$-labeling of DsbB and deuterium/hydrogen (D/H) exchange. For overexpression of perdeuterated DsbB, maintaining the cell growth rate is critical. Freshly transformed colonies were cultured in 20 mL minimal medium. When the OD_{600nm} reached 0.5, cells were pelleted and resuspended into 120 mL deuterated minimal medium (D_2O, ^{15}N ammonium sulfate, $^{2}H,^{13}C$-Glucose, and $^{2}H,^{13}C,^{15}N$-Bioexpress-1000). When the OD_{600nm} reached 0.5 again, cells were pelleted and resuspended into 800 mL deuterated minimal medium. Induction and purification are carried out as described above. Yields of perdeuterated DsbB are slightly lower than unlabeled DsbB. For the production of U-[$^{2}H,^{13}C,^{15}N$], Ile-δ1-[$^{13}CH_3$] and Val,Leu-[$^{13}CH_3,^{13}CH_3$] samples, Bioexpress-1000 was removed from the deuterated minimal medium, and 50mg/L of 2-keto-3-d2-1,2,3,4-13C-butyrate and 100mg/L of 2-keto-3-methyl-13C-3-d1-1,2,3,4-13C-butyrate (Cambridge Isotop Laboratories) (Tugarinov et al., 2004) were added 1 hour before induction.

For amide D/H exchange, purified DsbB was diluted to 50 μM with TRIS/NaCl buffer containing 1g/L DPC. DPC and SDS were added to a final concentration of 10 mM each,

resulting in partial unfolding of DsbB (Otzen, 2003). This DsbB solution was incubated at 30 ºC overnight to achieve complete D/H exchange. SDS was removed by loading DsbB onto a Ni-NTA column and washing extensively with TRIS/NaCl buffer with 1g/L DPC.

Preparation of perdeuterated UQ-free DsbB. The coding sequence for His_6-tagged DsbB was inserted into the pQE60 vector (Qiagen). The pQE60 based expression vector and a repressor plasmid pRep4 (Qiagen) were cotransformed into *E. coli ubiA menA* double mutant strain AN384 (Inaba et al., 2004; Wallace and Young, 1977). Cells were initially cultured in 20 mL minimal medium supplemented with 1.0 mM p-hydroxybenzoate (PHB). The rest of the growth, induction, and purification are the same as for perdeuterated DsbB with the exception that PHB was not included in the subsequent two culture steps. Yields of perdeuterated UQ-free DsbB are ~1 mg purified protein per liter of culture.

Methyl resonance assignments. Ile, Leu, and Val methyl assignments were achieved using a HMCM[CG]CBCA experiment and 3D [^{13}C-F_1, ^{13}C-F_2]-edited NOESY (200ms mixing time) (Tugarinov and Kay, 2003) on a 1.5 mM U-[^{2}H], Ile-δ1-[$^{13}CH_3$] and Val,Leu-[$^{13}CH_3$,$^{13}CH_3$]-labeled DsbB[CSSC] sample in deuterated DPC micelles. Methyl groups in all 8 Ile(δ1), 14 Val, and 14 out of 28 Leu sidechains were assigned. The missing assignments of half of the leucine methyls are primarily due to the low sensitivity

of the HMCM[CG]CBCA experiment. Another reason for incomplete leucine methyl assignments is the extensive chemical shift degeneracy of Leu Cα/Cβ pairs in α-helical membrane proteins. For example, all six leucines, except Leu25, in TM1 facing outside the protein, where there is a relatively homogeneous chemical environment of detergents had Cα and Cβ chemical shifts within 0.8 ppm of one another (see chemical shifts deposited in BMRB database). To confirm the leucine methyl NOE assignments, the eight leucine long-range and medium-range NOEs were checked against the ensemble of DsbB structures calculated without using these restraints.

Relaxation measurements. ^{15}N-{^{1}H} heteronuclear NOEs were measured using a TROSY based experiment (Zhu et al., 2000) with a 1.0 mM ^{2}H,^{15}N-labeled DsbB[CSSC] sample.

DsbA titration experiments. [^{15}N, ^{1}H] TROSY-HSQC experiments were used to monitor the DsbB chemical shift perturbations upon DsbA binding. Spectra were recorded on a 1.0 mM ^{2}H,^{15}N-labeled DsbB[CSSC] sample in the absence and in the presence of 1.5 mM unlabeled DsbA (C30S; C33S), (DsbA[SS]). Assignment was achieved by comparison of the two spectra.

Saturation transfer experiments. Saturation transfer experiments (Takahashi et al., 2000) were performed using a 4 ppm bandwidth WURST2 proton decoupling shape centered at

2 ppm for 1.5s. For alternate fids, the center of the WURST2 pulse was placed at 2 ppm and -81 ppm to switch on and off the aliphatic proton saturation. The difference spectra showing perturbed resonances were obtained by subtraction of the corresponding fids. To indentify saturation transfer from residual protons of deuterated DPC to DsbB, cross saturation transfer experiments were performed on two samples. One contained 0.2 mM ^{2}H, ^{13}C, ^{15}N DsbB[CSSC] in deuterated DPC. The second contained 0.4 mM ^{2}H, ^{13}C, ^{15}N DsbB[CSSC] and 2.0 mM unlabeled DsbA[SS] in deuterated DPC (Figure 4C, 4D and S9). The difference of the two spectra shows the saturation transfer from DsbA to DsbB.

DsbB-UQ2 resonance assignments. Proton chemical shifts of UQ10 in isotropic liquid phase have been assigned (Ondarroa and Quinn, 1986). Comparison with the proton chemical shifts of UQ2 in deuterated DPC micelles made it possible to assign resonances of the two methoxy groups (degenerate) at 3.97 ppm and the resonances of the 7-methylene at 3.18ppm. It also made it possible to group the remaining resonances: (a) 8-vinyl CH and 13-vinyl CH at around 5 ppm; (b) 11, 12-methylene and 5' methyl at around 2.0 ppm; (c) 10,15,16-methyl groups at ~1.6 ppm. In order to obtain unequivocal assignments for UQ-2, a 2D ^{1}H homonuclear NOESY spectrum (150ms mixing time) was collected on a 0.4 mM ^{2}H,^{13}C,^{15}N-labeled UQ-free DsbB[CSSC] sample supplemented with 2.0 mM UQ2 in deuterated DPC micelles. Only one set of resonances was observed for UQ2, indicating that UQ2 is in fast exchange between the DsbB-bound and unbound states. Based on the NOESY data, we were able to obtain a complete assignment for UQ2

with the exception of the 11- and 12-methylenes (Figure S8).

Assignment of the backbone amide resonances of UQ2-DsbB[CSSC] was achieved by comparison of TROSY-HSQC spectra of DsbB[CSSC] with UQ2 and UQ8. These assignments were subsequently validated using TROSY-based 3D HNCA and HN(CO)CA experiments.

NOE data collection. NOEs between backbone amide protons, methyl protons and tryptophan amide protons were recorded using three dimensional ^{15}N-edited, ^{13}C-edited, [^{15}N-F_1, ^{15}N-F_2]-edited, and [^{13}C-F_1, ^{13}C-F_2]-edited NOESY spectra with mixing times of 200, 200, 250, and 200 ms, respectively, on the same sample of U-[^{2}H], Ile-δ1-[$^{13}CH_3$] and Val,Leu-[$^{13}CH_3$, $^{13}CH_3$]-labeled DsbB[CSSC]. ^{15}N-edited and [^{15}N-F_1, ^{15}N-F_2]-edited NOESY spectra were manually assigned and categorized based on volume into four distance ranges: 1.8-2.9, 1.8-4.3, 1.8-4.9, 1.8-5.5 Å. The classification was based on known distances of (i,i+1), (i,i+2), and (i,i+3) backbone amide protons in α helices in high resolution crystal structures. NOEs involving methyl groups have an additional 0.5 Å allowance at the upper bound.

Structure calculations for DsbB. Structure calculations were carried out using simulated annealing protocols with XPLOR-NIH (Schwieters et al., 2003). Calculation of the

structure of DsbB was done in two steps. In the first step, the structure of each secondary structural element was determined to high resolution. The structures of these elements were then fixed by hydrogen bond restraints where appropriate and relatively tight backbone dihedral angle restraints. In a second step, these segments were folded together with RDCs, PREs and long-range NOE restraints.

Based on chemical shift derived backbone dihedral angles from TALOS (Cornilescu et al., 1999), DsbB[CSSC] was subdivided into four segments: (a) H1 and TM1 (aa1-38), (b) TM2 and TM3 (aa41-99), (c) PL2, H2, and PL2' (aa106-128), (d) PL2', S1, S2, and TM4 (aa132-166). Each segment was folded from random coil to high resolution by backbone dihedral angles, RDCs, sequential and medium range NOEs, and a few long-range NOEs. In the initial high temperature run at 3000 K and timestep of 10 fs, conformational energy terms were fixed: force constants for NOEs, $^{1}D_{NH}$ RDCs, and torsion angle restraints are 20 kcal mol^{-1} $Å^{-2}$, 0.005 kcal mol^{-1} Hz^{-2}, and 5 kcal mol^{-1} rad^{-2}, respectively. The empirical energy terms are ramped to their final values in 50 steps: the van der Waals radii from 0.4 to 0.8 of their regular value, k(vdw) = 0.004 -> 4.0 kcal mol^{-1} $Å^{-2}$, k(angle) = 0.4->1.0 kcal mol^{-1} $degree^{-2}$, and k(improper) = 0.4 -> 1.0 kcal mol^{-1} $degree^{-2}$. In the subsequent cooling steps, the bath temperature was lowered from 3000 K to 100 K in 25 K decrements. The empirical energy terms remain at their final values from the high temperature steps. Force constants for NOEs and $^{1}D_{NH}$ RDCs were ramped from 20 -> 30 kcal mol^{-1} $Å^{-2}$ and 0.005 -> 0.5 kcal mol^{-1} Hz^{-2}, respectively. The force constant for

torsion angle restraints was set to 200 kcal mol^{-1} rad^{-2}. $^{1}D_{NC'}$ and $1D_{C'Ca}$ RDC force constants were fixed to 0.8 and 0.4 times the value of the $^{1}D_{HN}$ RDC force constant in both high temperature and cooling steps. For each segment, 20 structures were calculated and 10 structures of lowest total energy were used to represent their ensemble conformation.

Hydrogen bonds were identified from ensemble structures of each segment by the following criteria: (a) hydrogen-acceptor oxygen distance (R_{HO}) is less than 2.4 Å, (b) angle of proton-donor-acceptor (θ_{HNO}) is less than 40 degrees, and (c) hydrogen bond is observed in more than 7 out of 10 structures. These calculated hydrogen bonds were validated using two criteria: (a) residues involved must be in a TALOS predicted regular secondary structure element and (b) the amide proton temperature coefficient ($\Delta\sigma(HN)/\Delta T$) is larger than –4.6 ppb K^{-1} (Cierpicki et al., 2002). The amide proton temperature coefficients were measured from TROSY-HSQC experiments at 25, 30, 35, 40, and 45 ºC. Both distance and geometry restraints were enforced for hydrogen bonded atoms in subsequent calculations (Lipsitz et al., 2002). Each segment was refined again using the same script with hydrogen bond distance restraints included. Mean backbone dihedral angles of ensemble structures were calculated using MOLMOL (Koradi et al., 1996). In regular secondary structure regions, these were subsequently used to replace the TALOS-derived dihedral angle restraints with a 15-degree error range.

To generate initial structures of full length DsbB[CSSC], a random coil was folded using NOEs, PREs, hydrogen bond, and backbone dihedral angle restraints. The initial high temperature step was run at 2000 K for 48,000 steps of 3 fs each. The force constant for van der Waals interaction, torsion angle restraints, and hydrogen bond geometry restraints were set to 0.002 kcal mol^{-1} $Å^{-2}$, 5 kcal mol^{-1} rad^{-2}, and 100 kcal mol^{-1} $Å^{-6}$, respectively. NOE, PRE, and hydrogen bond distance restraints were enforced by soft-square potentials and their force constants were fixed at 50 kcal mol^{-1} $Å^{-2}$, 5 kcal mol^{-1} $Å^{-2}$, and 50 kcal mol^{-1} $Å^{-2}$, respectively. In the subsequent cooling steps, the bath temperature was lowered from 2000 K to 100 K in 25 K decrements, using 316 time steps of 3 fs each. Van der Waals radii were ramped from 0.9 to 0.8 times their regular value and the van der Waals force constant was ramped from 0.003 to 4 kcal mol^{-1} $Å^{-2}$. The force constant for torsion angle restraints was increase to 200 kcal mol^{-1} rad^{-2}. NOEs, PREs, hydrogen bond distance, and hydrogen bond geometry terms remained the same. 100 initial structures were generated and 39 structures of lowest energy were subject to refinement. The same script and energy terms were used for refinement except that the PRE force constant was increased to 20 kcal mol^{-1} $Å^{-2}$ and RDC restraints were used. In the high temperature steps, the $^{1}D_{HN}$ RDCs force constant was fixed at 0.005 kcal mol^{-1} Hz^{-2}. In the cooling steps, the $^{1}D_{HN}$ RDCs force constant was ramped from 0.005 to 0.5 kcal mol^{-1} Hz^{-2}. $^{1}D_{NC'}$ and $^{1}D_{C'Ca}$ RDC force constants were fixed at 0.8 and 0.4 times the value of the $^{1}D_{HN}$ RDC force constant. From each of the 39 initial structures, three structures were generated. In each case, the structure of lowest total energy was selected as the refined

structure, resulting in a total of 39 refined structures. From the 39 refined structures, 20 structures of lowest total energy were chosen to represent the ensemble conformation of DsbB[CSSC].

Structure calculations for the DsbB[CSSC]-UQ2 complex. Structure calculations for the DsbB[CSSC]-UQ2 complex were essentially the same as the structure refinement of DsbB[CSSC] itself. Intermolecular NOEs, intramolecular NOEs of UQ2, and the intermolecular PRE of the UQ2 5' methyl group were used and their force constants are the same as previous NOE and PRE terms. The 39 lowest energy structures of DsbB[CSSC] and a UQ2 in an energy minimized conformation were used as initial structures. Five structures were generated from each initial structure and the structure of lowest total energy in each case was chosen as the refined structure. From these 39 refined structures, 20 structures of lowest energy which satisfy the intermolecular PRE restraints were selected to represent the ensemble conformation of the DsbB[CSSC]-UQ2 complex.

EPR measurements and docking of DsbB[CSSC] into POPC bilayer

Eleven MTSSL (R1) spin-labeled DsbB mutants (A14R1, L23R1, L30R1, G56R1, V72R1, L87R1, Q122R1, L137R1, A152R1, V161R1, and A163R1) were reconstituted in POPC vesicles by dialysis. Distances of these residues to the phosphate group region of the lipid bilayer were determined using the EPR power saturation technique. Briefly,

samples were placed in gas-permeable TPX tubes, and saturation of the resonance was carried out with a microwave power that varied from 0.25 to 63 mW. During these experiments, either a stream of air (oxygen accessibility) or nitrogen (baseline measurement and metal relaxing agent) was used to purge samples. The $P_{1/2}$ values, which are related to the product $(T_{1e}T_{2e})^{-1}$, were determined from the power saturation curves as described previously (Altenbach et al., 1989). The $P_{1/2}$ values were used in turn to determine the collision parameter Π for each reagent. The parameter Π is related to the change in T1e of the nitroxide and to its frequency of collision of with either nickel acetylacetone (NiAA, 20 mM in sample) or O_2 (~20% in air). For sites located deep within the bilayer, O_2 accessibility (and thus collision frequency) is greater than that for NiAA due to the non-polar nature of the oxygen molecule. On the other hand, residues located near the lipidic/aqueous interface have an increased accessibility for NiAA. The membrane depth parameter, Φ, was determined from the ratios of the Π values for each reagent as described previously (Altenbach et al., 1996). The distance between each nitroxide nitrogen and the nearest phosphate group plane was obtained from the Φ values using the calibration curve determined previously (Altenbach et al., 1994).

The spin label depths in the bilayer obtained from EPR data were used with XPLOR-NIH to determine DsbB orientation with respect to the lipid bilayer in the following way. The DsbB residues indicated above were changed to cysteines and MTSSL groups were attached. Twenty starting structures were generated by allowing all

DsbB sidechains to undergo simulated annealing and energy minimization; backbone atoms were fixed in the NMR structure positions. Subsequently, two planes were generated 37.8 Å apart representing the phosphate-to-phosphate distance in POPC (Lewis and Engelman, 1983), and spin label point-to-plane harmonic potentials were applied during simulated annealing and energy minimization to orient DsbB relative to the two planes. The selection of which phosphate plane is nearest to each spin label was done visually prior to simulated annealing and energy minimization; depths from orientation calculations were then measured. For each of the 20 generated structures, the sum of the differences between the calculated and the experimentally determined distances for each of the seven nitroxide nitrogens to the corresponding nearest phosphate plane was obtained. The average of these 20 resulting sums was 44.2 ± 7.0 Å. The structure with the lowest sum (31.0 Å) was selected to represent the orientation of DsbB within the bilayer (Figures 3A and 3B). For comparison, Figure S7 shows depths measured using the EPR method and saturation transfer effects from the DPC detergent to DsbB measured using NMR, showing good agreement between these two measurements obtained using different techniques and in different environments (micelle and bilayer).

Modeling of DsbB-DsbA complex. The crystal structure of DsbB(Cys130Ser)-DsbA(Cys33Ala) (PDB code 2HI7) and the solution structure of DsbB[CSSC] were superimposed by overlapping backbone atoms of the DsbB

transmembrane domain (aa 15-33, 42-52, 71-96, 143-159) using the program MOLMOL.

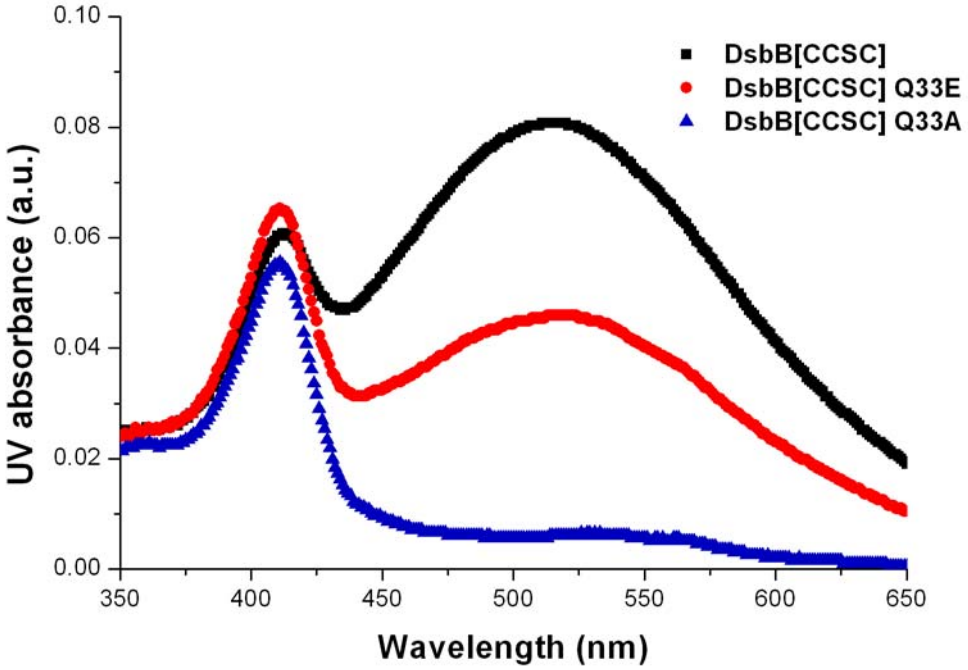

Figure S1. UV absorbance of DsbB[CCSC] Q33 mutants.

Q33A mutant of DsbB[CCSC] shows significantly reduced UV absorbance at 510 nm. The UV absorbance of DsbB[CCSC] or its mutants was recorded from 250 nm to 650 nm in 25 mM TRIS (pH 8.0), 50 mM KCl buffer with 50 mM DPC. Absorbance curves were scaled that the A_{280nm} equals 1.0 to compensate the concentration differences between samples.

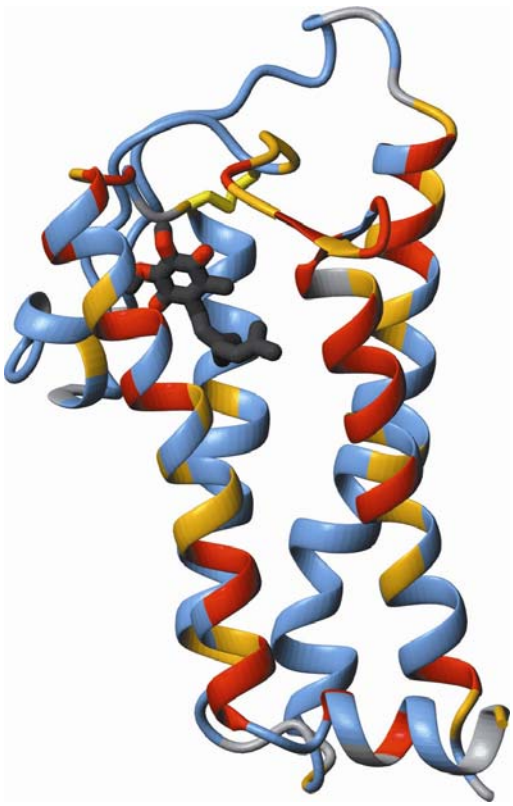

Figure S2.Chemical shift differences suggest the isoprenoid tail of ubiquinone-8 packs between TM1 and TM4 of DsbB.

Mapping the chemical shift differences between UQ8 and UQ2-loaded DsbB[CSSC] onto the DsbB-UQ2 complex structure suggests that the isoprenoid tail of UQ8 packs between TM1 and TM4. Strong (>40 Hz), medium (20-40 Hz), and weak (0-20 Hz) changes are colored red, yellow, and blue, respectively. Residues with no information are colored gray.

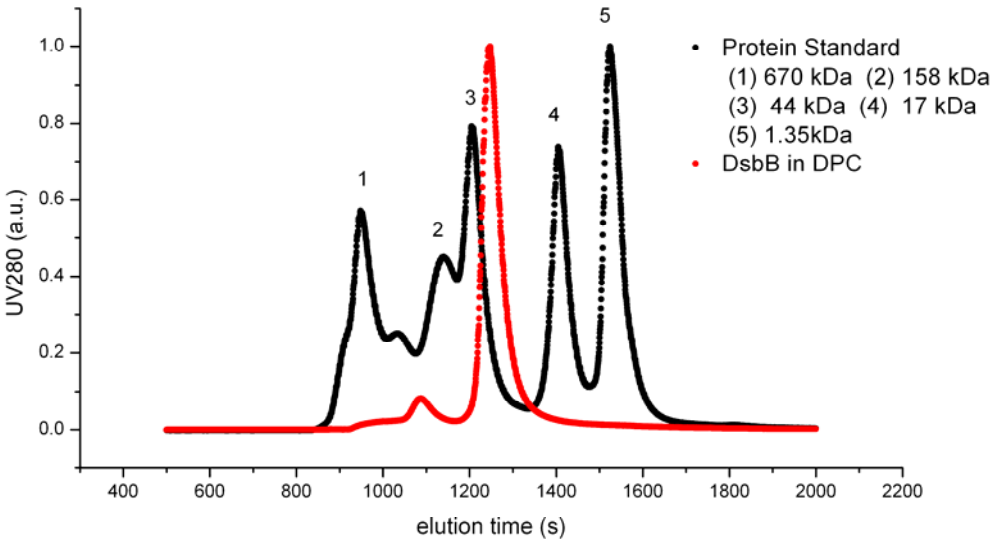

Figure S3. Size exclusion chromatography shows DsbB is a monomer in DPC.

Elution profiles of DsbB[CSSC] in 10g/L DPC (red) and Bio-Rad gel filtration standard (black) run on a Bio-Silect SEC 250-5 column. The UV absorbance is scaled such that the peak height of the highest peak in each profile equals one.

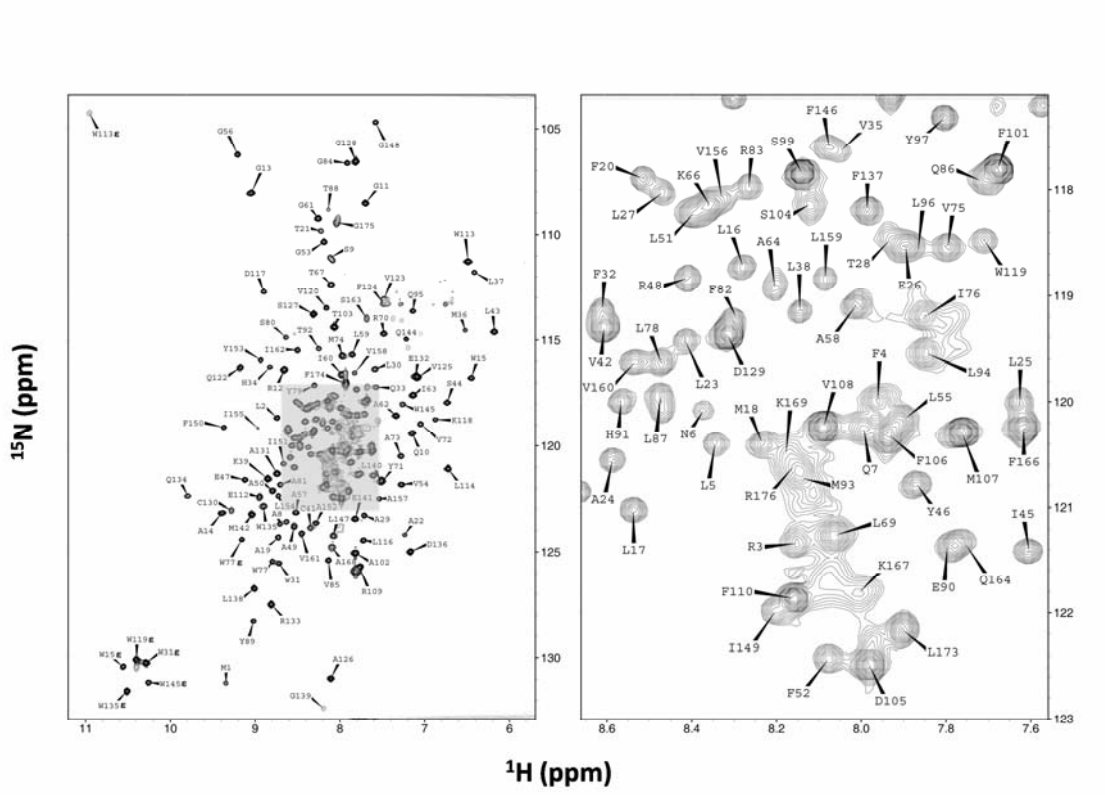

Figure S4. DsbB resonance assignments.

TROSY-HSQC spectrum of a 1.2 mM ^{2}H, ^{13}C,^{15}N-labeled DsbB[CSSC] sample in DPC micelles collected on a Varian Inova 600 MHz NMR spectrometer at 40º C.

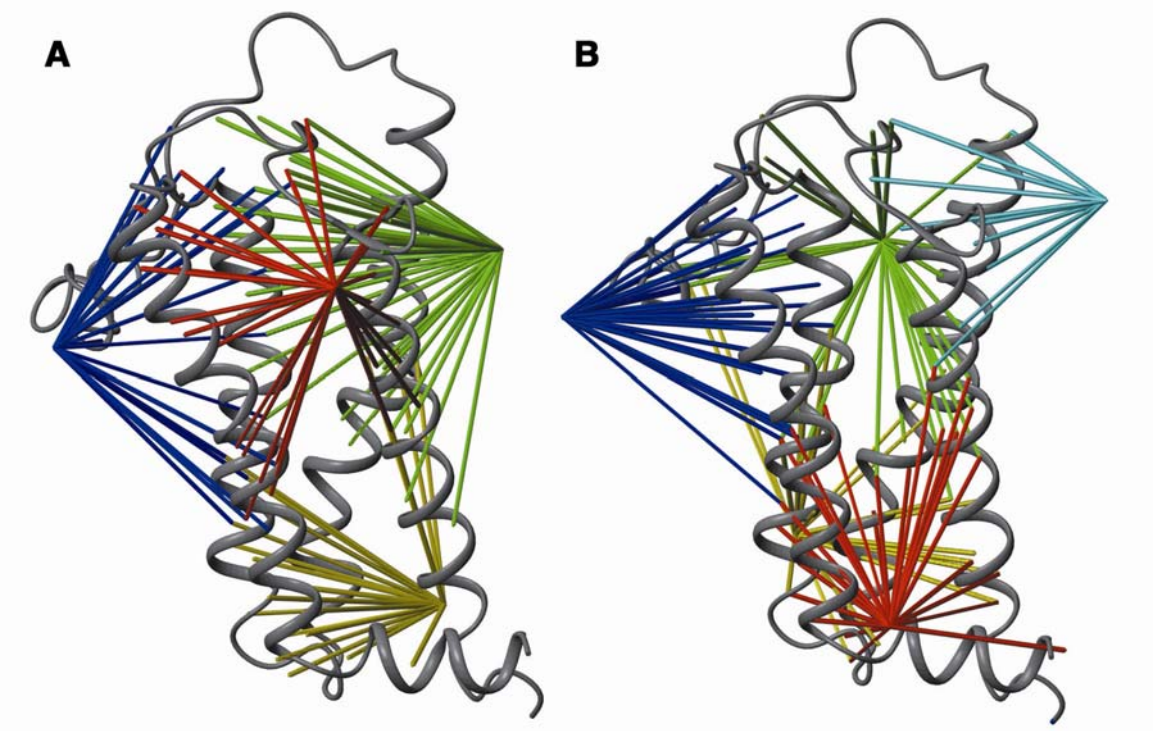

Figure S5. PRE restraints.

PRE restraints derived from nine MTSSL labeled DSbB[CSSC] samples. Distances with both upper and lower bounds from Leu30Cys-MTSSL (blue), Phe137Cys-MTSSL (red), Tyr89Cys-MTSSL (green), and Val161Cys-MTSSL (yellow) spin labels to backbone amide protons are shown in Panel A. Distances from Gln122Cys-MTSSL (blue), Leu87Cys-MTSSL (green), Gly139Cys-MTSSL (cyan), Val72Cys-MTSSL (yellow), and Ala14Cys-MTSSL (red) are shown in Panel B.

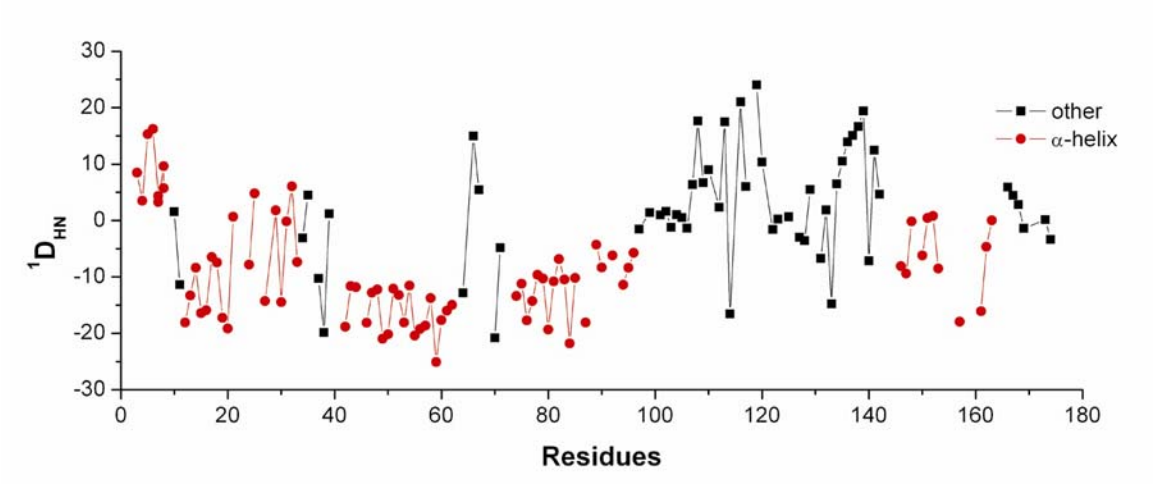

Figure S6. Plot of $^1D_{HN}$ dipolar couplings versus the primary sequence.

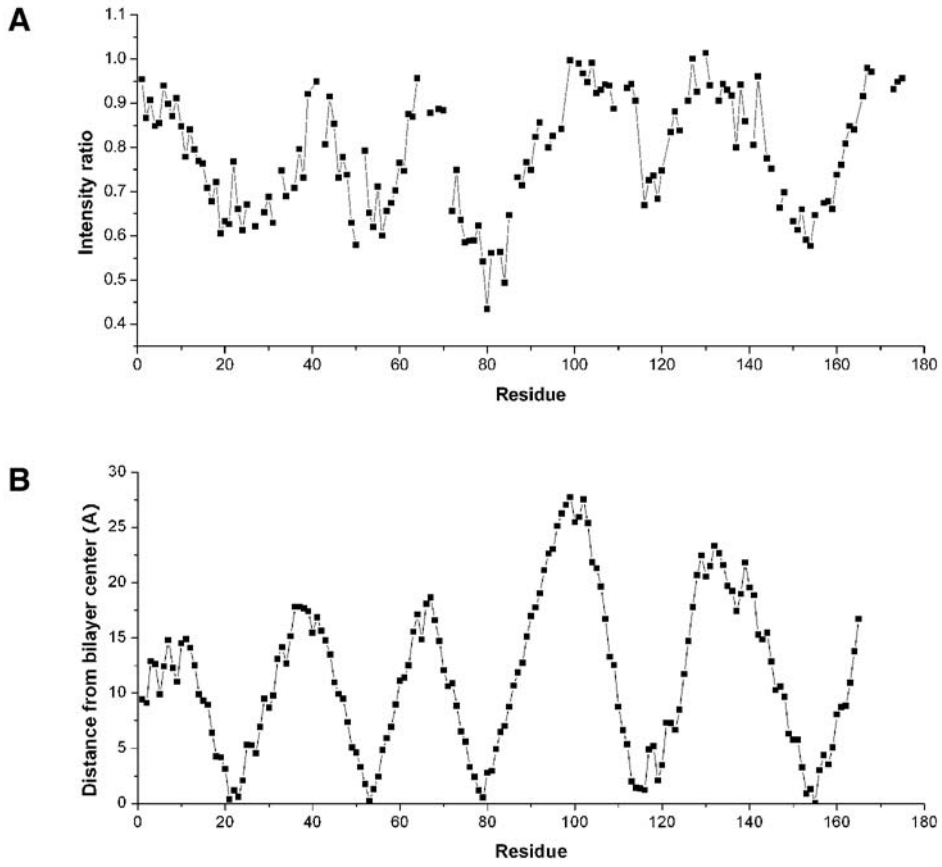

Figure S7. DsbB transmembrane depth measurements.

(A) Amide proton attenuation due to saturation transfer between DPC and DsbB (Chill et al., 2006). Plot shows the intensity ratio of amide signals in the presence and absence of a 1.5s proton saturation pulse (0.35-1.85 ppm) applied on the DPC aliphatic chain ($C^{2\text{-}11}H_2$ and $C^{12}H_3$) for a time of 1.5 sec. (B) Distance between DsbB backbone Cα atoms and POPC bilayer central plane derived from EPR membrane depth measurements.

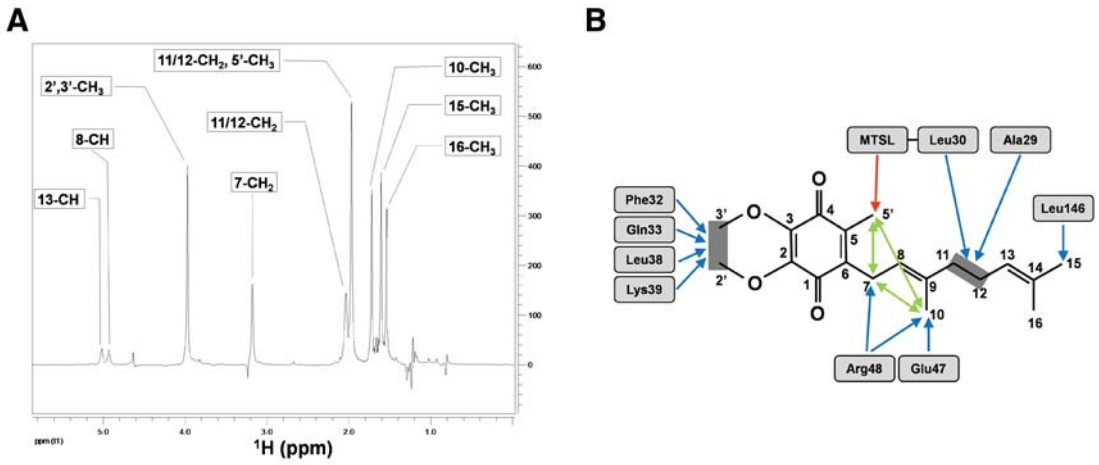

Figure S8. UQ2 assignment and UQ2-DsbB interaction.

(A) 1D ^{1}H NMR spectrum of 2.0 mM UQ2 in 20g/L deuterated DPC micelle and D_2O buffer. The residual proton signals from deuterated DPC have been subtracted out using a sample without UQ2. (B) UQ2 structure and summary of inter (blue) and intra (green) UQ2 NOEs and PREs (red) used in structure calculation of DsbB-UQ2 complex. Spins with chemical shift degeneracy are covered by gray shadows.

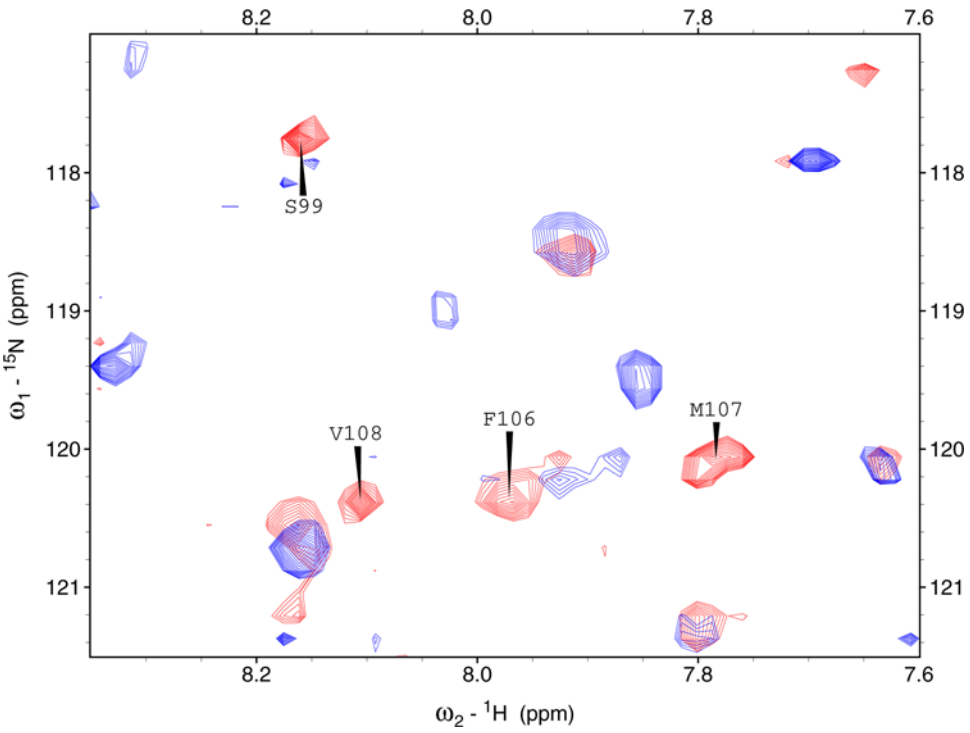

Figure S9. Saturation transfer between DsbA and DsbB.

Overlay of two saturation transfer difference spectra for DsbB[CSSC]. Blue spectrum was recorded on a 0.2 mM ^{2}H, ^{13}C, ^{15}N DsbB[CSSC] sample in deuterated DPC. Blue peaks represent the saturation transfer from residual protons of deuterated DPC to DsbB[CSSC]. Red spectrum was recorded on a 0.4 mM ^{2}H, ^{13}C, ^{15}N DsbB[CSSC] and 2.0 mM unlabeled DsbA[SS] sample in deuterated DPC. Red peaks represent the saturation transfer from protons of both DsbA[SS] and deuterated DPC to DsbB[CSSC]. Peaks only appearing in the red spectrum are labeled with residue number. These peaks correspond to saturation transfer from DsbA[SS] to DsbB[CSSC].

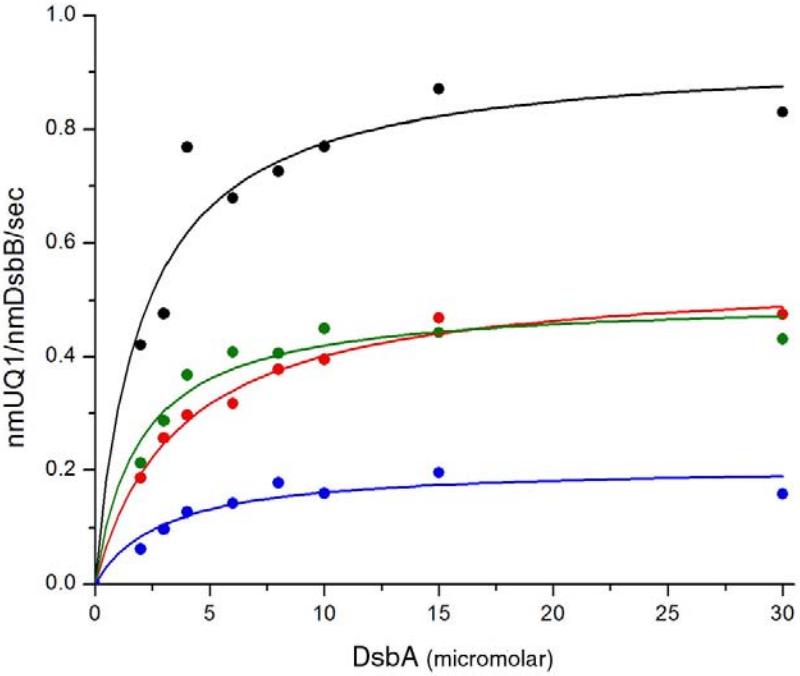

	K_m (μM for DsbA)	K_{cat} (sec^{-1})
Wild type	**2.06 ± 0.64**	**0.93 ± 0.07**
G128A	**3.65 ± 0.42**	**0.55 ± 0.02**
D129A	**1.95 ± 0.48**	**0.50 ± 0.03**
D129L	**2.93 ± 1.09**	**0.21 ± 0.02**

Figure S10. Mutation on PL2' reduces DsbB activity.

Michaelis-Menten parameters for wild type DsbB (black), G128A (red), D129A (olive), and D129L (blue) were determined by monitoring the UV absorbance signal for UQ reduction (Bader et al., 2000). The reaction buffer is 50 mM sodium phosphate (pH 6.0), 300 mM NaCl, 0.1% dodecyl-β-D-maltoside and 40 μM UQ1.

Supplemental references

Altenbach, C., Flitsch, S. L., Khorana, H. G., and Hubbell, W. L. (1989). Structural studies on transmembrane proteins. 2. Spin labeling of bacteriorhodopsin mutants at unique cysteines. Biochemistry *28*, 7806-7812.

Altenbach, C., Greenhalgh, D. A., Khorana, H. G., and Hubbell, W. L. (1994). A collision gradient method to determine the immersion depth of nitroxides in lipid bilayers: application to spin-labeled mutants of bacteriorhodopsin. Proc. Natl. Acad. Sci. U.S.A. *91*, 1667-1671.

Altenbach, C., Yang, K., Farrens, D. L., Farahbakhsh, Z. T., Khorana, H. G., and Hubbell, W. L. (1996). Structural features and light-dependent changes in the cytoplasmic interhelical E-F loop region of rhodopsin: a site-directed spin-labeling study. Biochemistry *35*, 12470-12478.

Bader, M. W., Xie, T., Yu, C. A., and Bardwell, J. C. (2000). Disulfide bonds are generated by quinone reduction. J. Biol. Chem. *275*, 26082-26088.

Chill, J. H., Louis, J. M., Miller, C., and Bax, A. (2006). NMR study of the tetrameric KcsA potassium channel in detergent micelles. Protein Sci. *15*, 684-698.

Cierpicki, T., Zhukov, I., Byrd, R. A., and Otlewski, J. (2002). Hydrogen bonds in human ubiquitin reflected in temperature coefficients of amide protons. J. Magn. Reson. *157*, 178-180.

Cornilescu, G., Delaglio, F., and Bax, A. (1999). Protein backbone angle restraints from searching a database for chemical shift and sequence homology. J. Biomol. NMR, *13*, 289-302.

Inaba, K., Takahashi, Y. H., Fujieda, N., Kano, K., Miyoshi, H., and Ito, K. (2004). DsbB elicits a red-shift of bound ubiquinone during the catalysis of DsbA oxidation. J. Biol. Chem. *279*, 6761-6768.

Koradi, R., Billeter, M., and Wüthrich, K. (1996). MOLMOL: a program for display and analysis of macromolecular structures. J. Mol. Graphics. *14*, 51-55.

Lewis, B. A., and Engelman, D. M. (1983). Lipid bilayer thickness varies linearly with acyl chain length in fluid phosphatidylcholine vesicles. J. Mol. Biol. *166*, 211-217.

Lipsitz, R. S., Sharma, Y., Brooks, B. R., and Tjandr, N. (2002). Hydrogen bonding in high-resolution protein structures: a new method to assess NMR protein geometry. J. Am. Chem. Soc. *124*, 10621-10626.

Ondarroa, M., and Quinn, P. J. (1986). Proton magnetic resonance spectroscopic studies of the interaction of ubiquinone-10 with phospholipid model membranes. Eur. J. Biochem. *155*, 353-361.

Otzen, D. E. (2003). Folding of DsbB in mixed micelles: a kinetic analysis of the stability of a bacterial membrane protein. J. Mol. Biol. *330*, 641-649.

Schwieters, C. D., Kuszewski, J. J., Tjandra, N. and Clore, G. M. (2003). The Xplor-NIH NMR molecular structure determination package. J. Magn. Reson. *160*, 66-74.

Takahashi, H., Nakanishi, T., Kami, K., Arata, Y., and Shimada, I. (2000). A novel NMR method for determining the interfaces of large protein-protein complexes. Nat. Struct. Biol. *7*, 220-223.

Tugarinov, V., Hwang, P. M., and Kay, L. E. (2004). Nuclear magnetic resonance spectroscopy of high-molecular-weight proteins. Annu. Rev. Biochem. *73*, 107-146.

Tugarinov, V., and Kay, L. E. (2003). Ile, Leu, and Val methyl assignments of the 723-residue malate synthase G using a new labeling strategy and novel NMR methods. J. Am. Chem. Soc. *125*, 13868-13878.

Wallace, B. J., and Young, I. G. (1977). Role of quinones in electron transport to oxygen and nitrate in Escherichia coli. Studies with a ubiA- menA- double quinone mutant. Biochim. Biophys. Acta. *461*, 84-100.

Zhu, G., Xia, Y., Nicholson, L. K., and Sze, K. H. (2000). Protein dynamics measurements by TROSY-based NMR experiments. J. Magn. Reson. *143*, 423-426.